

# Influence of the nanocellulose raw material characteristics on the electrochemical and mechanical properties of conductive paper electrodes

A. Mihranyan · M. Esmaili · A. Razaq ·  
D. Alexeichik · T. Lindström

Received: 19 December 2011 / Accepted: 28 January 2012 / Published online: 23 February 2012  
© Springer Science+Business Media, LLC 2012

**Abstract** Paper-based conductive electrode materials of polypyrrole (PPy) and nanocellulose (NC) have received much attention lately for applications in non-metal-based energy storage devices, ion exchange, etc. The aim of this study was to study how the primary characteristics of NC raw materials impact and electrochemical properties of conductive NC–PPy composite sheets. Three NC raw materials were used: Cladophora cellulose (NC<sub>UU</sub>) produced at Uppsala University, Cladophora cellulose (NC<sub>FMC</sub>) produced at FMC Biopolymer, and microfibrillated cellulose (NC<sub>INN</sub>) produced at Innventia AB. Composite paper sheets of PPy coated on the substrate NC material were produced. The NC raw materials and the composites were characterized with a battery of techniques to derive their degree of crystallinity, degree of polymerization, specific surface area, pore size distribution, porosity, electron conductivity, charge capacity and tensile properties. It was found that the pore size distribution and overall porosity increase upon coating of NC fibres for all the samples. The charge capacity of the

composites was found to decrease with the porosity of the samples. It was further found that the mechanical strength of the pristine NC sheets was largely dependent on the overall porosity, with NC<sub>INN</sub> having the highest mechanical strength and lowest porosity in the series. The mechanical properties of the composite NC–PPy sheets were significantly diminished as compared with pristine NC sheets because of the impaired H-bonding between fibres and PPy-coated nanofibres. It was concluded that to improve the mechanical properties of PPy–NC sheets, a fraction of additive bare NC fibres is beneficial. Future study may include the effect of both soluble and insoluble additives to improve the mechanical strength of PPy–NC sheets.

## Introduction

Polypyrrole (PPy) is one of the most commonly investigated conductive polymers. Relatively high charge capacity, capability of straightforward synthesis, possibility of chemical as well as electrochemical polymerization and coating over different kinds of substrates are some of the most notable features of PPy [1]. However, PPy suffers from several drawbacks such as poor cycling stabilities [2–4], low accessible degree of doping [5, 6], high self-discharge rates [7, 8], and mass transport limitations in thick polymer layers [4]. Furthermore, its large scale industrial applicability is limited because of brittleness and poor post-synthesis processability, such as poor solubility in most solvents, poor heat-annealing properties, and poor compactability, which makes it hard to produce coherent, self-standing films, wires, or other moulded or cast forms [9].

In situ polymerization of pyrrole (Py) monomers on various substrates has been widely used to render PPy with the preferred mechanical properties [10–15]. In this

---

A. Mihranyan (✉) · M. Esmaili · A. Razaq  
Nanotechnology and Functional Materials, Department  
of Engineering Sciences, Ångström Laboratory, Uppsala  
University, P. O. Box 534, 75121 Uppsala, Sweden  
e-mail: albert.mihranyan@angstrom.uu.se

### Present Address:

A. Razaq  
Physics Department, COMSATS Institute of Information  
Technology, Lahore 54000, Pakistan

D. Alexeichik  
FMC BioPolymer, 1301 Oglethown Road, Newark,  
DE 19711, USA

T. Lindström  
Innventia AB, Drottning Kristinas Väg 55, 114 86 Stockholm,  
Sweden

respect, both conductive, e.g. metals [16–18] or carbon [4, 19, 20] materials, and non-conductive substrates, e.g. synthetic [21–23] or natural polymers [24–26], have been used. Cellulose is known for its excellent mechanical properties and bears enormous industrial value. It is inexpensive, lightweight, non-toxic and biodegradable, and it also originates from renewable sources. Furthermore, cellulose, unlike wool [24] or silk [25, 26], exhibits high affinity to be coated with PPy, which is believed to be because of direct interactions between OH-groups abundantly present on cellulose surface and NH-groups of Py ring [11, 13]. Paper-like composites of cellulose and PPy have recently received much attention as environmental-friendly electrode materials for non-metal-based energy storage devices [27, 28] as well as high capacity electrode materials for electrochemically controlled ion exchange [29–34]. Further, these conductive paper materials have been used as a substrate to be coated with various metals including silver for antibacterial disposable paper products [13].

Cellulose exists in a variety of crystalline forms, e.g. cellulose I $\beta$  and I–IV, and even different allomorphs for the same crystalline phase, e.g. cellulose I $\alpha$ . Furthermore, cellulose can be obtained from different sources which include terrestrial plants, algae, bacteria, fungi and even aquatic animals such as tunicates [35]. Depending on the source and the processing, the cellulose materials exhibit different degrees of crystallinity (DC), degrees of polymerization (DP), specific surface areas, porosities, fibre thicknesses, etc., which are all important for ensuring the mechanical strength of paper.

The various aspects of coating of cellulose with conductive polymers were summarized in the recently published reviews [1, 36]. The effects of micron-thick cellulose fibres used by the paper industry, such as type of the pulp, fibre length, fines' content and fibre curl, on the conductivity of cellulose composites with PPy have been investigated [37]. It was shown that types of cellulose pulp and degree of curl are trivial, but the amount of fines and fibre length are important for producing composites of PPy and cellulose. It was suggested that with shortening of the fibre length and raising the fine's fraction, the conductivity of the composite increases, but this also impairs the conductive network continuity in the composite [37]. It was further shown that inclusion of small amounts of cellulose whiskers improves the mechanical properties of PPy, i.e. producing increased tensile strength and Young's modulus, as well as reduced elongation at break [38].

During the last decade, nanocellulose (NC) materials have been intensively investigated for their exceptional mechanical properties [35, 39–41]. The use of NC is advantageous because NC not only provides necessary

mechanical strength but also features large surface area, which is favourable to obtain large charge capacity in paper-like electrodes. Not surprisingly, NCs from algae [42], wood [43, 44] and bacteria [45, 46] have all been used to be coated with conductive polymers. In this respect, the so-called salt-and-paper battery, based on NC from *Cladophora* algae and PPy, is exemplary and shows great promise in the development of environmental-friendly, non-metal-based energy storage devices [1, 27, 28, 47, 48]. While the investigations on the improvement of the electrochemical performance of the paper-based energy storage devices are currently underway, the importance of the NC component has been somewhat overlooked. In particular, systematic studies on the influence of the primary characteristics of the NC raw materials as substrates for producing conductive paper electrodes are lacking. The aim of this study is thus to study how the primary characteristics of NC raw materials impact on the mechanical and electrochemical properties of conductive NC–PPy composite sheets.

## Experimental

### Materials

Py, iron (III) chloride, hydrochloric acid, sodium chloride and Tween-80 were purchased from Sigma Aldrich, Germany. Two batches of NC from *Cladophora* algae were used: NC<sub>UU</sub> produced at Uppsala University as earlier described [49] and NC<sub>FMC</sub> as delivered by FMC Biopolymer (batch G3095-10), USA, having a hemicellulose's content of less than 1%. The NC<sub>INN</sub> was manufactured at Innventia, Stockholm. A bleached sulphite softwood cellulose pulp (Domsjö ECO Bright; Domsjö Fabriker AB) consisting of 40% pine (*Pinus sylvestris*) and 60% spruce (*Picea abies*) with hemicellulose content of 13.8% (measured as solubility in 18% NaOH, R1830) and a lignin content of 1% (estimated to 0.165\*Kappa number, SCAN C 1:00) was used as a source for the microfibrillated cellulose. The pulp was used in its never-dried form. The phosphate buffer used during the enzymatic treatment was prepared from 11 mM KH<sub>2</sub>PO<sub>4</sub> and 9 mM Na<sub>2</sub>HPO<sub>4</sub> so that pH was between 6.8 and 7.2, and the monocomponent endoglucanase enzyme (Novozym 476, Novozym A/S) was used without further purification. To a pulp slurry with 4% fibre consistency, 0.83 ECU/g fibres of the enzyme was added. The enzymatic treatment temperature was 50 °C for 2 h, and then the pulp was treated at 90 °C for 40 min to inactivate the enzyme. The product was then defibrillated using high shear mechanical homogenization. The characteristics of NC<sub>INN</sub> have been reported in a previous publication [50].

### Pristine NC sheets

A 0.5 wt% dispersion of NC was dispersed in deionized water using a high-energy ultrasonicator (VibraCell 750 W, Sonics, USA) for 10 min. The dispersion of NC was then collected on a filter paper in a Buchner funnel and dried in ambient air to make a paper sheet.

### Composite NC–PPy sheets

300 mg of NC (dry weight) was dispersed in 60 ml of deionized water for 10 min using a high-energy ultrasonicator (VibraCell 750W, Sonics, USA). Then, the NC dispersion was mixed with 50 ml of HCl (0.5 M) solution containing 1.5 ml Py and a drop of Tween-80 and stirred with a magnetic stirrer for 5 min. Simultaneously 12.6 g FeCl<sub>3</sub> was dissolved in 100 ml HCl (0.5 M) and then added to the NC–Py mixture to induce polymerization. The mixture was placed inside a fume-hood for 40 min under stirring and then washed with 5 l of HCl (0.5 M) in a Buchner funnel on a filter (Whatman filter paper 42, 90 mm, Cat No. 1442 090) followed by 1 l of NaCl (0.1 M). The filter cake was then transferred to a beaker with 100 ml of deionized water and sonicated for 2 min to re-disperse the composite fibres. The well-dispersed suspension was finally transferred in a Buchner funnel and drained. The final product was dried in ambient air, and fixed between metal plates with clutches to produce a composite sheet. The samples were stored in ambient conditions before characterization.

In order to investigate the effect of inclusion of bare NC fibres on the composite's mechanical properties after polymerization, the following procedure was carried out. A composite of NC<sub>UU</sub>PPy was formed as described above. Following rinsing, the NC<sub>UU</sub>PPy composite was mixed with NC<sub>INN</sub> dispersion (2.26 wt%), so that the final added NC<sub>INN</sub> (dry) contents were 12, 35, and 52 wt% composite. The mixture was blended using a mechanical homogenizer (IKA T25 Ultra-Turrax, Germany) at 6000 rpm for 10 min. Before homogenization, each NC<sub>INN</sub> batch was dispersed for 10 min in 100 ml of deionized water using a high-energy ultrasonicator (VibraCell 750W, Sonics, USA). The mixture was then drained on a filter (Whatman filter paper 42, 90 mm, Cat No. 1442 090) to form a filter cake, which was subsequently dried in ambient air, fixed between metal plates, to form a sheet.

## Methods

### Scanning electron microscopy (SEM)

The SEM images were taken with a Leo Gemini 1550 FEG SEM (UK) instrument. The surface of the sheets was sputtered with Pt–Au to reduce artefacts because of

charging. The materials were mounted on adhesive tapes over aluminium stubs.

### Degree of crystallinity (DC)

The X-ray diffractograms were obtained using a diffractometer D5000 (Siemens, Germany) instrument. CuK<sub>α1</sub> radiation was used ( $\lambda = 0.154$  nm), and the  $2\theta$  angle was adjusted between 10 and 30°.

The DC was measured as follows:

$$\text{DC}\% = \frac{I_{\text{cr}} - I_{\text{am}}}{I_{\text{cr}}} \times 100 \quad (1)$$

where,  $I_{\text{cr}}$  stands for the peak intensity at around  $2\theta = 22^\circ$  and  $I_{\text{am}}$  is the baseline at  $2\theta = 18^\circ$  [51].

### Degree of polymerization (DP)

The DP was obtained from the relative viscosity of the NC samples in a Cuene solution as described in the ASTM standard method D1795 [52]. The relative viscosity was obtained at different dilutions using a capillary viscometer (Cannon–Fenske 100, USA). The viscosity ( $\eta$ ) was calculated in centipoises, as follows:

$$\eta = Ct\rho \quad (2)$$

where,  $C$  = viscometer constant,  $t$  = outflow time (s) and  $\rho$  = density (g/ml). The relative viscosity ( $\eta_{\text{rel}}$ ) was calculated as follows:

$$\eta_{\text{rel}} = \frac{\eta}{\eta_0} \quad (3)$$

where  $\eta_0$  is the viscosity of the solvent.

The values of intrinsic viscosity  $\eta$  were obtained by plotting  $\log\left[\frac{\eta_{\text{rel}}-1}{c}\right]$  against  $c$  for four concentrations and extrapolating the straight line through the points to  $c = 0$ . The intercept gave us  $\log[\eta]$ . A reasonably good approximation to DP is obtained by multiplying intrinsic viscosity by 190 [52].

### Specific surface area and pore size distribution

N<sub>2</sub> gas adsorption and desorption isotherms were obtained using an ASAP 2020 (Micromeritics, USA) instrument. The BET specific surface area and the density function theory (DFT) pore size distribution curves were derived from the isotherms using the ASAP 2020 (Micromeritics, USA) software.

### True density and porosity

The true density of the samples was measured using a He-pycnometer (AccuPyc1340, Micromeritics, USA).

The porosity of the samples was measured according to the following formula:

$$\varepsilon\% = \left(1 - \frac{\rho_B}{\rho_T}\right) \times 100 \quad (4)$$

where,  $\varepsilon\%$  is the porosity,  $\rho_B$  is the bulk density and  $\rho_T$  is the true density. The bulk density was obtained from the dimensions of the samples as

$$\rho_B = \frac{m}{V} \quad (5)$$

where,  $V$  is the volume, and  $m$  is the weight of the sample.

### Electrical conductivity

I–V sweep method was used to estimate the bulk resistance of the dried composite sheets at room temperature using a semiconductor analyser device (B1500A, Agilent Technologies, USA). The sample conductivity was estimated as follows:

$$\sigma = \left(\frac{\Delta I}{\Delta U}\right) \times \left(\frac{L}{wd}\right) \quad (6)$$

where  $\left(\frac{\Delta I}{\Delta U}\right) = \frac{1}{R}$  stands for the conductance of the sample obtained from the slope of the current versus voltage curve,  $L$  is the length,  $w$  is the width, and  $d$  is the thickness of the sample. The selected sample dimensions were approximately about  $12 \times 5 \times 0.7 \text{ mm}^3$ . Both the ends of the sample were painted with silver paint to ensure of good electrical contacts with the needle probes. The measurements were taken within a week from the date of synthesis.

### Cyclic voltammetry

Cyclic voltammetry was performed in a standard 3-electrode electrochemical cell at room temperature at a scan rate of 5 mV/s using an Autolab/GPES interface (ECO Chemie, The Netherlands). The composite sheets were employed as the working electrode, a coiled Pt wire was used as the counter electrode, and an Ag/AgCl electrode was used as the reference electrode. 2 M NaCl solution was used as the electrolyte. The potential region was adjusted so as to ensure that overoxidation of the sample was avoided. The charge capacity of composites was calculated from the area-under-curve of the oxidation current.

### Mechanical testing

The mechanical properties of the samples were measured in an axial tensile mode using a tensile strength analyser (MiniMat, Rheometric Scientific Inc, USA). The experiments were performed in a room with controlled relative humidity (50%) at 25 °C. Strips of the sample were cut

with scissors having the following dimensions: 60 × (3–5) mm. The thickness, depending on the sample, varied between 0.03 and 0.05 mm for pristine NC samples, and between 0.55 and 1.25 mm for the composites. The tensile strength, tensile index, yield stress and Young's modulus were derived.

## Results and discussion

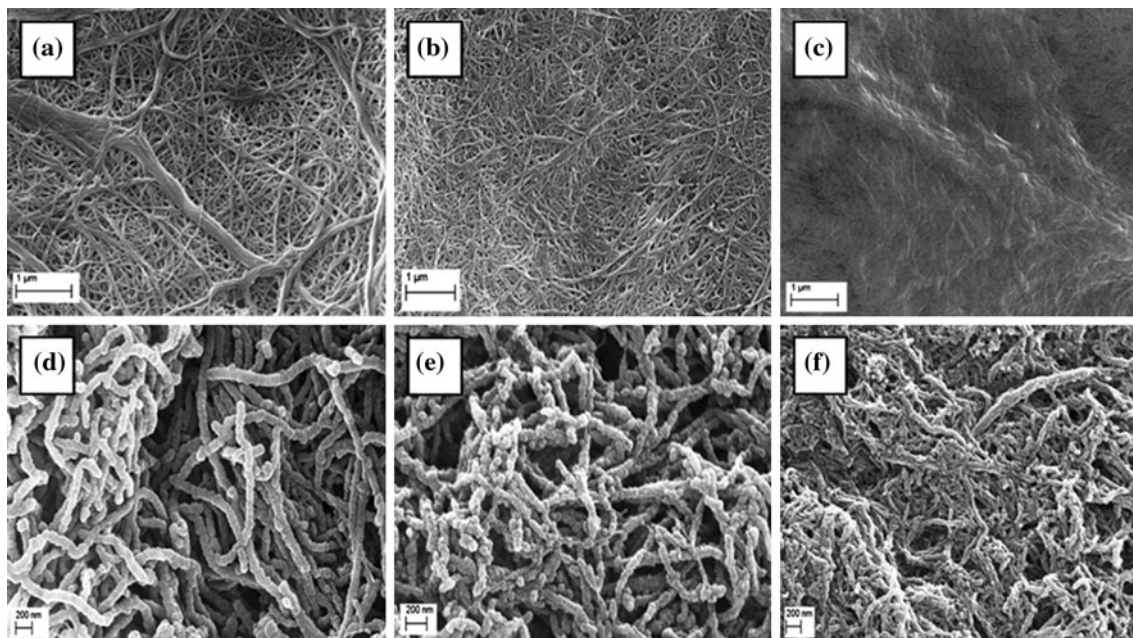
### Primary characteristics

Figure 1 shows the internal structure of the produced samples as observed in SEM. In Fig. 1a–c, the micrographs of the pristine NC sheets are shown.

It is seen from these images that NC<sub>UU</sub> sample (Fig. 1a) consisted of a network of fine cellulose nanofibres, which were often aggregated into cellulose bundles. No bundles were seen in NC<sub>FMC</sub> (Fig. 1b), which consisted of fine nanofibres featuring an intertwined network. In NC<sub>INN</sub> sample (Fig. 1c), no nanofibre network similar to that seen in Fig. 1a–b was observed, and the images suggested a dense, non-porous structure. The thicknesses of the individual NC–PPy nanofibres were about 100 nm, as observed by SEM.

In Fig. 1d–f, the SEM micrographs of the composite NC–PPy samples are shown. In all the samples, worm-like structures of individual composite nanofibres with somewhat uneven surfaces were seen. In all the samples, bare fibres or partially coated cellulose nanofibres were not detected. Compared with the pristine NC<sub>UU</sub> sample (Fig. 1a), no bundles were observed in the composite NC<sub>UU</sub>PPy sample (Fig. 1d). The most obvious differences were observed in the NC<sub>INN</sub>PPy sample (Fig. 1f) as compared with NC<sub>INN</sub> sample (Fig. 1c): in Fig. 1f, a porous structure of intertwined composite nanofibres is seen, whereas the image in Fig. 1c suggests a dense, non-porous structure. It is also observed that the structure of NC<sub>INN</sub>PPy, although somewhat denser, is generally similar to that seen for NC<sub>UU</sub>PPy and NC<sub>FMC</sub>PPy in Fig. 4d–e, suggesting the presence of an open, loose structure.

Figure 2 depicts the X-ray powder diffractograms of the pristine NC samples, reflecting the batch-to-batch variability with respect to amorphous content. It is seen from Fig. 2 that the NC<sub>UU</sub> and NC<sub>FMC</sub> show nearly identical diffractograms and are featured with markedly sharp and highly distinct Bragg peaks, especially in the region between 14 and 17 (2θ), which is typical for highly crystalline algae cellulose [35, 53]. The NC<sub>INN</sub> sample, which originates from wood sources, exhibits a remarkably different XRD profile concordant with wood cellulose diffractograms described earlier: A broad halo is observed for the 2θ region between 14 and 17 (2θ) [54]. It is also seen



**Fig. 1** SEM images of pristine NC and composite NC-PPy sheets: **a** NC<sub>UU</sub>, **b** NC<sub>FMC</sub>, **c** NC<sub>INN</sub>, **d** NC<sub>UU</sub>PPy, **e** NC<sub>FMC</sub>PPy, and **f** NC<sub>INN</sub>PPy

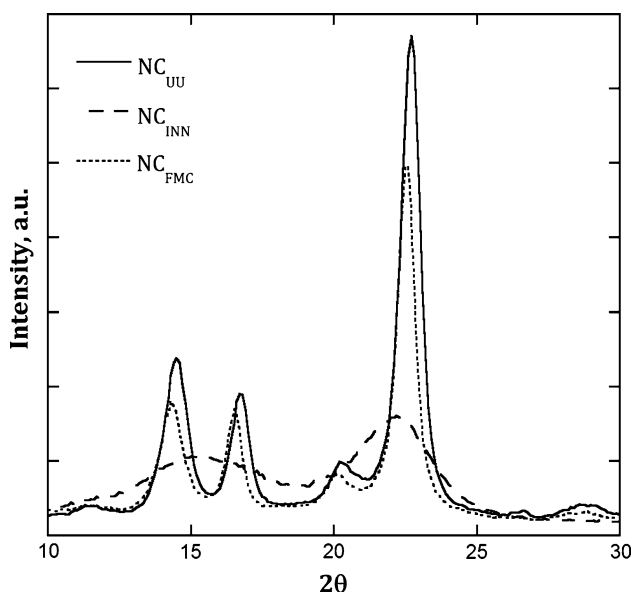


**Fig. 2** XRD patterns of NC<sub>UU</sub>, NC<sub>FMC</sub>, and NC<sub>INN</sub> samples

that the peak at 22 degrees ( $2\theta$ ) (i.e. major cellulose I peak) is much broader for NC<sub>INN</sub> sample than those for NC<sub>FMC</sub> and NC<sub>UU</sub>, which suggests a more disordered structure in the former sample. The results are in full accordance with the reported profiles for NC materials from algae and wood sources [35, 53].

Table 1 summarizes the primary characteristics of the samples. The DP of NC<sub>UU</sub>, NC<sub>FMC</sub>, and NC<sub>INN</sub> samples were 1647, 742, and 335, respectively, whereas DC values of NC<sub>UU</sub>, NC<sub>FMC</sub>, and NC<sub>INN</sub> samples were, respectively,

estimated to be 94, 92, and 59%. Thus, it can be concluded that, while NC<sub>UU</sub> and NC<sub>FMC</sub> were featured with nearly identical DC, the cellulose wood-based nanofibres had a lower DC compared to Cladophora nanofibres. Owing to insoluble nature of PPy, DP values of NC in the composites following the polymerization could not be determined. It should, however, be noted that the effect of acidic hydrolysis, which occurs almost exclusively in the amorphous regions of cellulose, on DP is tangible at elevated temperatures [55]. Earlier TEM analysis images clearly showed the presence of NC core inside individual PPy-NC nanofibres, suggesting that NC fibres are predominantly intact, which is further supported by the tubular shape of PPy-NC nanofibres seen in SEM [27, 33, 42, 43]. It is further seen from Table 1 that there is a substantial difference between the surface areas of NC<sub>INN</sub> and the other two NC samples as was expected, and observed from the SEM images shown in Fig. 4a–c. The values of surface area of pristine NC<sub>UU</sub> and NC<sub>FMC</sub> sheets were around 90 m<sup>2</sup>/g, whereas that for NC<sub>INN</sub> sheet was less than 0.5 m<sup>2</sup>/g, and the latter could not be measured with N<sub>2</sub> gas adsorption. This is because of the large differences between the cross-sectional areas of elemental Cladophora nanofibres (20–30 nm) and the elemental wood-based nanofibres having a diameter of around 5 nm [35]. Owing to the higher stiffness of Cladophora-based nanofibres, the surface tension forces (Campbell forces) cannot consolidate the structure during drying, resulting in a much higher porosity of nanostructures based on Cladophora-based nanofibres.

It is seen from Table 1 that the true density values for NC<sub>UU</sub> and NC<sub>FMC</sub> samples are slightly higher than that for

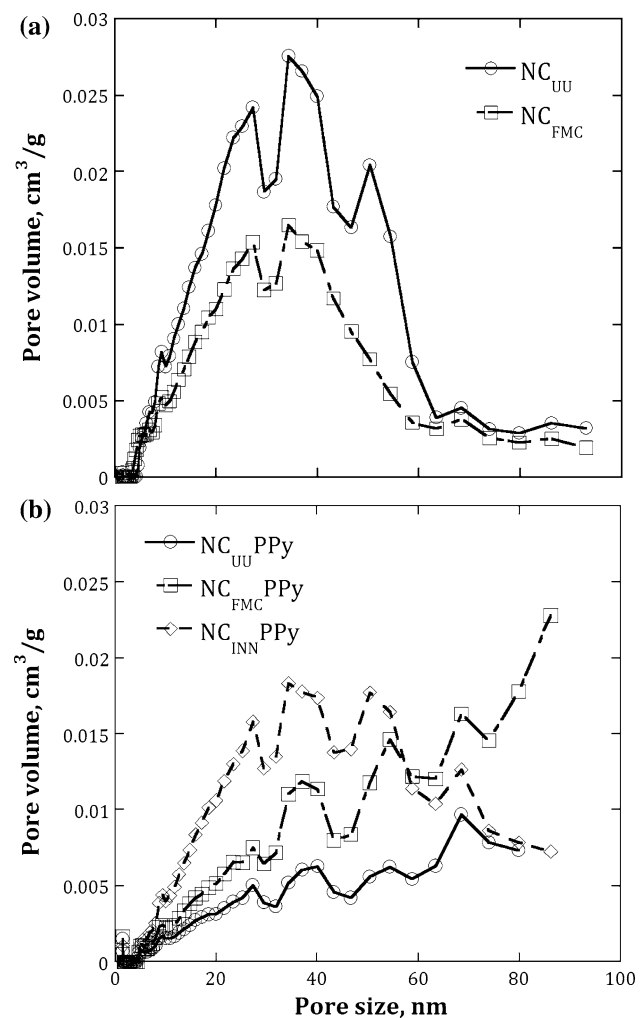
NC<sub>INN</sub> sample. The latter has also been observed earlier, and it is due to the higher DC of Cladophora cellulose [35]. The true density values of the composite samples were between 1.60 and 1.65 g/cm<sup>3</sup>, which is comparable with the previously reported data [56]. It should also be noted that values of true density for cellulose reported in the literature vary between 1.51 and 1.67 g/cm<sup>3</sup> [57]. It is clearly inferred from Table 1 that the composite samples were featured with higher porosity than the corresponding pristine NC samples: NC<sub>UU</sub>PPy sample showed a smaller specific surface area than NC<sub>FMC</sub>PPy; however, the porosities of NC<sub>UU</sub>PPy and NC<sub>FMC</sub>PPy were relatively similar.

Figure 3 shows the pore size distribution curves of the samples studied (note that owing to the low surface area of NC<sub>INN</sub> sample, the N<sub>2</sub> gas adsorption/desorption curves could not be obtained for it). It is seen from Fig. 3 that pores in NC<sub>UU</sub> and NC<sub>FMC</sub> samples are predominantly in the range between 10 and 50 nm. Upon coating the NC fibres with PPy, it becomes evident that the distribution of pores for NC<sub>UU</sub>PPy and NC<sub>FMC</sub>PPy samples is shifted towards larger pore sizes approaching 100 nm. The broad distribution of pores and their shift to larger sizes agree well with the SEM images, cf. Fig. 1d, e. It should further be noted that the pore volume of NC<sub>INN</sub>PPy sample appears to be substantially smaller than those for NC<sub>UU</sub>PPy and NC<sub>FMC</sub>PPy samples.

#### Electrochemical properties

The conductivity values of the composites are summarized in Table 1. The average value of conductivity for NC<sub>INN</sub>PPy was 4.3 S/cm, whilst those for NC<sub>UU</sub>PPy and NC<sub>FMC</sub>PPy were 2.9 and 2.8 S/cm, respectively. It could be speculated that better conductivity of NC<sub>INN</sub>PPy sample is due to somewhat lower porosity of this sample, which implies a denser network of conductive strands [37].

Figure 4a shows the cyclic voltammograms of the composites studied in 2 M NaCl electrolyte at a scan rate of 5 mV/s. In a typical cyclic voltammogram, the oxidation and reduction peaks correspond to the absorption and desorption of chloride ions into/from the composites,



**Fig. 3** DFT pore size distribution of **a** pristine NC and **b** PPy–NC sheets

respectively [42]. The cyclic voltammograms were then used to estimate the charge capacity of the composites.

Figure 4b shows the correlation between the charge capacity and the porosity of the composite NC–PPy samples. It is seen from this graph that the charge capacity increases with the overall porosity of the samples. It was previously suggested that the high surface area of the composite may be favourable to obtain greater

**Table 1** Primary characteristics of the pristine NC and composite NC–PPy sheets

Sample	DC (%)	DP	Surface area (m <sup>2</sup> /g)	True density (g/cm <sup>3</sup> )	Porosity (%)	Conductivity (S/cm)
NC <sub>UU</sub>	94	1647	90.5	1.60	43.2	–
NC <sub>FMC</sub>	92	742	89.9	1.64	36.7	–
NC <sub>INN</sub>	59	335	<0.5	1.58	3.6	–
NC <sub>UU</sub> PPy	–	–	60.0	1.65	75.3	2.9
NC <sub>FMC</sub> PPy	–	–	96.0	1.60	69.3	2.8
NC <sub>INN</sub> PPy	–	–	80.8	1.62	55.4	4.3

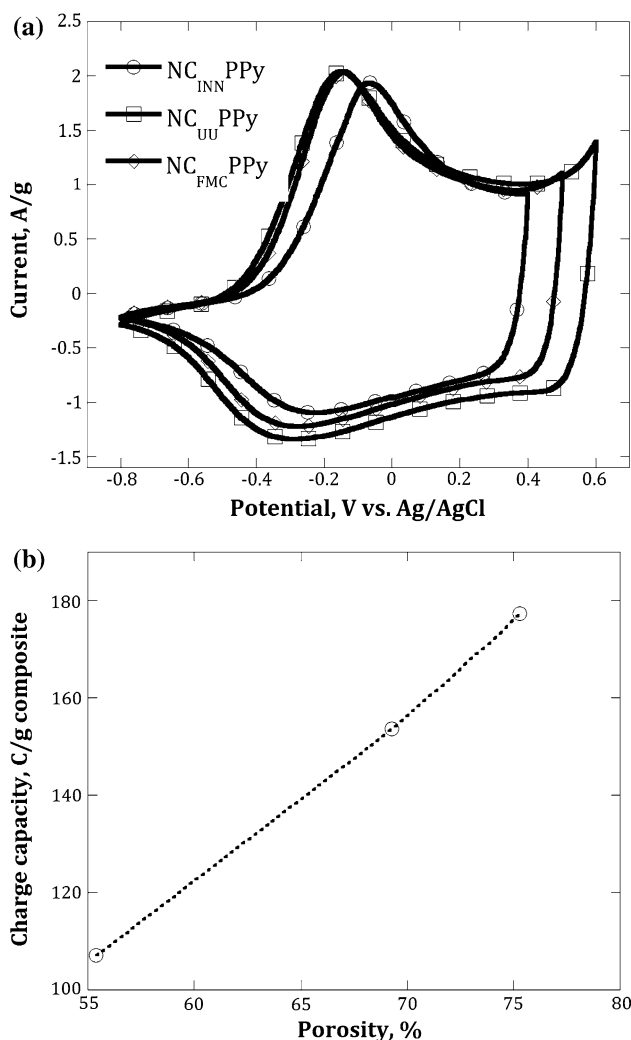


**Fig. 4** Electrochemical performance of the composite samples: **a** cyclic voltammograms of the composite NC–PPy samples and **b** charge capacity values versus overall porosity

ion-exchange capacity than for a composite with low surface area [42]. However, the influence of the overall porosity on the charge capacity has hitherto not been discussed. The NC<sub>UU</sub>PPy sample has larger overall porosity than NC<sub>FMC</sub>PPy sample, although the latter sample is featured with a larger surface area than the former one. The charge capacity, as seen from Fig. 4b, progressively decreases with the decrease in the overall porosity of the samples, whereas no correlation between the surface area and charge capacity could be established in the series studied. In this respect, even if the material may possess a large surface area, small pores and low porosity may also hinder the access of the electrolyte to the PPy-conductive strands during oxidation and reduction. Because the values of porosity of the composites are roughly in the same range, as opposed to the porosity values of the pristine NC sheets, it would be preferable to investigate the influence of

porosity as well as the pore size distribution on the charge capacity of the composite materials over a markedly broader range of values in the future.

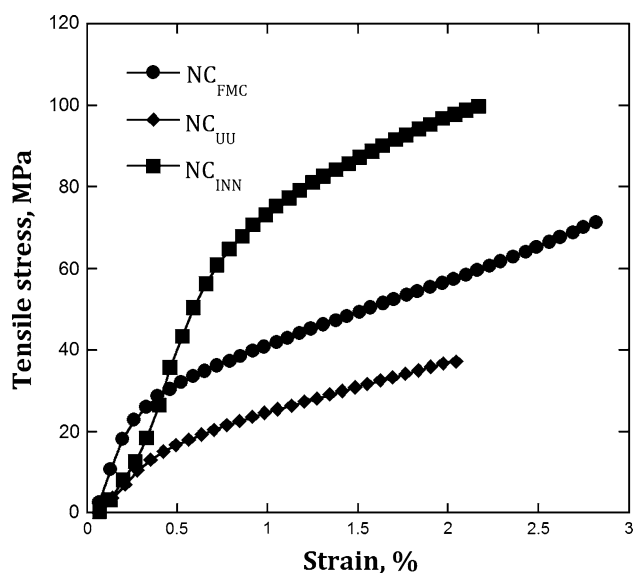
Mechanical properties

Figure 5 shows the typical stress versus strain curves of the pristine NC sheets. From such curves, the tensile strength (i.e. strength at break), tensile index (tensile strength normalized per bulk density), Young’s modulus and yield stress (i.e. the transition point from elastic to ductile behaviour) values were derived.

Table 2 summarizes the mechanical properties of the NC samples studied. Whilst the tensile strength values of NC<sub>INN</sub> sample are higher than those for NC<sub>FMC</sub> and, especially, for the NC<sub>UU</sub> sample, these differences are evened out when the bulk density of the pristine NC sheets is taken into account, indicating that probably the main reasons for the observed difference in the tensile strengths of pristine NC sheets are the variations in the porosity. The mechanical properties of NC<sub>INN</sub>-films have been reported before [58], and with the current DP of the films, the stress–strain curves are identical.

It is further seen from Table 2 that the tensile strength values for the composites were markedly lower, viz. ~50–100 times, for the composites compared with the pristine NC sheets. The composites were rather brittle, and the yield stress values could not be obtained, as there was no detectable transition point from elastic-to-ductile deformation.

It is commonly known that chemical polymerization of Py monomers using oxidants, such as iron (III) chloride, produces a powder product featured with very poor



**Fig. 5** Stress versus strain curves of the pristine NC sheets

**Table 2** Mechanical properties of the pristine NC and composite PPy–NC sheets

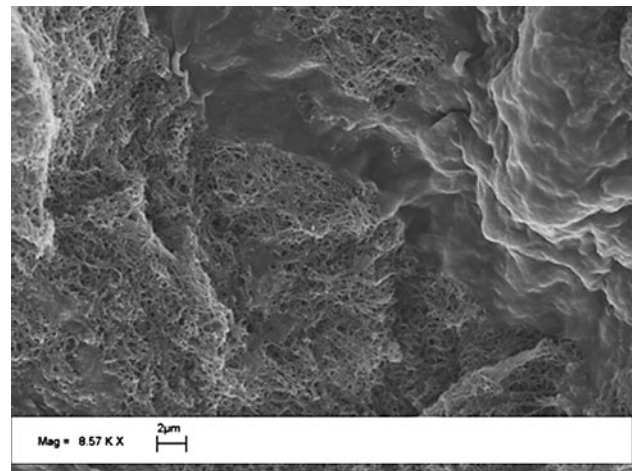
Sample	Tensile index (kNm/kg)	Tensile strength (MPa)	Young's modulus (GPa)	Yield stress (MPa)
NC <sub>UU</sub>	50	46	0.42	17
NC <sub>FMC</sub>	77	80	0.90	34
NC <sub>INN</sub>	74	112	1.13	77
NC <sub>UU</sub> PPy	3.2	1.3	0.01	–
NC <sub>FMC</sub> PPy	1.2	0.6	0.01	–
NC <sub>INN</sub> PPy	1.4	1.0	0.03	–

The results are the mean ( $n = 3$ ) with the standard deviation in the range between 7 and 14%

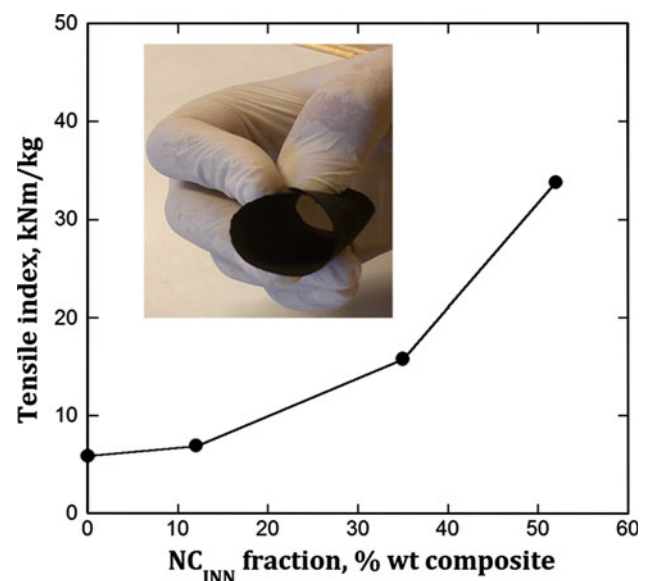
post-synthesis processability, such as poor solubility in most solvents, poor compatibility or poor heat-annealing properties [9]. Clearly, in situ polymerization of Py monomers on NC fibres enables production of self-standing paper sheets which can be moulded into any shape or cut with scissors. Thus, although the manufacturing of self-standing PPy sheets is enabled by making composites with NC, the tensile properties of composite samples are diminished as compared to pristine NC sheets.

Although the composite samples possess larger pores and are generally featured with higher porosity than pristine NC samples, this factor alone is not sufficient to explain the differences between the pristine NC and composite samples, since tensile index values of the composites are still almost an order of magnitude lower than those for the pristine NC sheets. It can therefore be suggested that the deterioration of the mechanical properties of the composites compared to the pristine NC samples could be due to the shielding of the H-bonds between the OH-groups present on the surfaces of cellulose adjacent nanofibres since PPy-to-PPy contacts are obviously much weaker. The OH-groups present on the cellulose nanofibres are occupied by interactions with the NH-groups of Py rings, which results in an uninterrupted and continuous PPy coating on individual NC fibres [11, 13]. The presence of the continuous and uninterrupted coating on NC fibres is critical for good electrical conductivity [42]; however, it tends to deteriorate the mechanical properties of otherwise strong pristine NC sheets. The fact that the composite samples exhibit relatively high porosities as compared with the pristine NC sheets could also be indicative of the impaired H-bondings between adjacent NC fibres, pointing to the limited shrinking upon drying.

From the above discussion, it is inferred that the mechanical properties of the composites would strongly benefit from the presence of limited amounts of bare NC fibres embedded in the matrix of the composite NC–PPy fibres. In order to verify this hypothesis, various

**Fig. 6** SEM image of highly porous composite NC<sub>UU</sub>PPy sample featuring islands of non-porous NC<sub>INN</sub> embedded into the matrix

proportions of bare NC<sub>INN</sub> fibres were post-synthetically added to the composite NC<sub>UU</sub>PPy which was then moulded into sheets. Figure 6 depicts an SEM image of such a sample, in which NC<sub>INN</sub> is seen as non-porous islands, which was post-synthetically embedded into the porous matrix of the NC<sub>UU</sub>PPy sample. The mechanical properties of the thus-produced composite sheets, featuring bare NC fibres as an additive, are presented in Fig. 7. It is seen from Fig. 7 that, upon inclusion of bare NC<sub>INN</sub> fibres to the NC<sub>UU</sub>PPy composite, the tensile index, which accounts for the differences in bulk density of the samples and, thereby, largely eliminates the effects of porosity, progressively

**Fig. 7** Influence of additive NC<sub>INN</sub> fibres on the tensile index of composite NC<sub>UU</sub>PPy samples. The inset in the graph depicts the composite sample with 52% added NC<sub>INN</sub> fraction



increases in direct proportion to the added fraction of NC<sub>INN</sub> fibres.

These results thus illustrate that the affinity between bare NC fibres is critical for the formation of the mechanically strong composites of NC–PPy. The reinforcing effects of water-soluble polymers such as xylan or carboxymethylcellulose on the mechanical properties of PPy–NC films have recently been shown [10, 59].

## Conclusions

The results of the present study suggest that coating the pristine NC fibres with PPy shifts the pore size distribution to larger pore sizes and produces composites featured with open, loosely packed structure of large surface areas. The composites exhibit good electroactivity which seems to be dependent on the total porosity of the composite. It was also observed that the mechanical strength of the composites is diminished in comparison with pristine NC samples. The observed effect was interpreted to be because of impaired H-bonding between adjacent pristine NC fibres. Post-synthetic inclusion of bare NC fibres to composites was found to enhance the mechanical properties of NC–PPy composites.

**Acknowledgements** Professor Kristofer Gamstedt, Department of Engineering Sciences, Uppsala University, is thanked for his valuable discussions and providing facilities for the mechanical tests. The financial supports from the Swedish Research Council (VR # 621-2009-4626), the Swedish Foundation for Strategic Research (SSF # RMA08-0025), and the Nordic Innovation Center (NICE, # 10014) are also gratefully acknowledged.

## References

- Nyholm L, Nyström G, Mihranyan A, Strømme M (2011) *Adv Mater* 23:3751. doi:10.1002/adma.201004134
- Naoi K, Morita M (2008) *Electrochem Soc Interface* 17:44
- Naoi K, Simon P (2008) *Electrochem Soc Interface* 17:34
- Kim JH, Lee YS, Sharma AK, Liu CG (2006) *Electrochim Acta* 52:1727. doi:10.1016/j.electacta.2006.02.059
- Snook GA, Kao P, Best AS (2011) *J Power Sources* 196:1. doi:10.1016/j.jpowsour.2010.06.084
- Katz HE, Searson PC, Poehler TO (2010) *J Mater Res* 25:1561. doi:10.1557/JMR.2010.0201
- Novak P, Muller K, Santhanam KSV, Haas O (1997) *Chem Rev* 97:207. doi:10.1021/cr941181o
- Liu CH, Meng CZ, Chen LZ, Hu CH, Fan SS (2010) *Nano Lett* 10:4025. doi:10.1021/nl1019672
- Qian RE (1993) *Conjugated polymers and related materials*. Oxford University Press, London
- Beneventi D, Sasso C, Zeno E et al (2010) *Macromol Mater Eng* 295:934. doi:10.1002/mame.201000148
- Johnston JH, Kelly FM, Moraes J, Borrmann T, Flynn D (2006) *Curr Appl Phys* 6:587. doi:10.1016/j.cap.2005.11.067
- Johnston JH, Moraes J, Borrmann T (2005) *Synth Met* 153:65. doi:10.1016/j.synthmet.2005.07.138
- Kelly FM, Johnston JH, Borrmann T, Richardson MJ (2007) *Eur J Inorg Chem* 35:5571. doi:10.1002/ejic.200700608
- Qian XR, Ding CY, Shen J, An XH (2010) *Bioresources* 5:303
- Qian XR, Ding CY, Yu G, An XH (2010) *Cellulose* 17:1067. doi:10.1007/s10570-010-9442-6
- Fan LZ, Maier J (2006) *Electrochem Commun* 8:937. doi:10.1016/j.elecom.2006.03.035
- Hara S, Zama T, Takashima W, Kaneto K (2004) *Synth Met* 146:47. doi:10.1016/j.synthmet.2004.06.021
- Chung HJ, Jung HH, Cho YS et al (2005) *Appl Phys Lett* 86:213113. doi:10.1063/1.1940125
- Woo SW, Dokko K, Kanamura K (2008) *J Power Sources* 185:1589. doi:10.1016/j.jpowsour.2008.08.035
- Muthulakshmi B, Kalpana D, Pitchumani S, Renganathan NG (2006) *J Power Sources* 158:1533. doi:10.1016/j.jpowsour.2005.10.013
- Wu J, Zhou D, Too CO, Wallace GG (2005) *Synth Met* 155:698. doi:10.1016/j.synthmet.2005.08.032
- Bhadani R, Baranwal PP, Bhadini SN (2002) *J Polym Mater* 19:259
- Varesano A, Antognozzi B, Tonin C (2010) *Synth Met* 160:1683. doi:10.1016/j.synthmet.2010.05.041
- Kelly FM, Johnston JH, Borrmann T, Richardson MJ (2008) *J Nanosci Nanotechnol* 8:1965. doi:10.1166/jnn.2008.040
- Cucchi I, Boschi A, Arosio C, Bertini F, Freddi G, Catellani M (2009) *Synth Met* 159:246. doi:10.1016/j.synthmet.2008.09.012
- Boschi A, Arosio C, Cucchi I, Bertini F, Catellani M, Freddi G (2008) *Fiber Polym* 9:698. doi:10.1007/s12221-008-0110-5
- Nyström G, Razaq A, Strømme M, Nyholm L, Mihranyan A (2009) *Nano Lett* 9:3635. doi:10.1021/NL901852h
- Olsson H, Nyström G, Strømme M, Sjödin M, Nyholm L (2011) *Electrochem Commun* 13:869. doi:10.1016/j.elecom.2011.05.024
- Razaq A, Strømme M, Nyholm L, Mihranyan A (2011) *ECS Trans* 35:135. doi:10.1149/1.3571986
- Gelin K, Mihranyan A, Razaq A, Nyholm L, Strømme M (2009) *Electrochim Acta* 54:3394. doi:10.1016/j.electacta.2009.01.010
- Razaq A, Mihranyan A, Welch K, Nyholm L, Strømme M (2009) *J Phys Chem B* 113:426. doi:10.1021/jp806517h
- Strømme M, Frenning G, Razaq A, Gelin K, Nyholm L, Mihranyan A (2009) *J Phys Chem B* 113:4582. doi:10.1021/jp9002627
- Rubino S, Razaq A, Nyholm L, Strømme M, Leifer K, Mihranyan A (2010) *J Phys Chem B* 114:13644. doi:10.1021/jp106317p
- Razaq A, Nyström G, Strømme M, Mihranyan A, Nyholm L (2011) *PLoS One* 6:e29243. doi:10.1371/journal.pone.0029243
- Mihranyan A (2011) *J Appl Polym Sci* 119:2449. doi:10.1002/app.32959
- Tobjörk D, Österbacka R (2011) *Adv Mater* 23:1935. doi:10.1002/adma.201004692
- Kang GJ, Ni YG (2008) 2nd International Papermaking and Environment Conference, Tianjin, China
- Weder C, van den Berg O, Capadona JR (2007) *Biomacromolecules* 8:1353. doi:10.1021/bm061104q
- Eichhorn SJ, Dufresne A, Aranguren M et al (2010) *J Mater Sci* 45:1. doi:10.1007/s10853-009-3874-0
- Siro I, Plackett D (2010) *Cellulose* 17:459. doi:10.1007/s10570-010-9405-y
- Klemm D, Kramer F, Moritz S et al (2011) *Angew Chem Int Ed* 50:5438. doi:10.1002/anie.201001273
- Mihranyan A, Nyholm L, Garcia Bennett AE, Strømme M (2008) *J Phys Chem B* 112:12249. doi:10.1021/jp805123w
- Nyström GM, Mihranyan A, Razaq A, Lindström T, Nyholm L, Strømme M (2010) *J Phys Chem B* 114:4178. doi:10.1021/jp911272m
- Liew SY, Thielemans W, Walsh DA (2010) *J Phys Chem C* 114:17926. doi:10.1021/jp3698p

45. Marins JA, Soares BG, Dahmouche K, Ribeiro SJL, Barud H, Bonemer D (2011) *Cellulose* 18:1285. doi:[10.1007/s10570-011-9565-4](https://doi.org/10.1007/s10570-011-9565-4)
46. Hu W, Chen S, Yang Z, Liu L, Wang H (2011) *J Phys Chem B* 115:8453. doi:[10.1021/jp204422v](https://doi.org/10.1021/jp204422v)
47. Razaq A, Nyholm L, Sjödin M, Strømme M, Mihranyan A (2012) *Adv Energy Mater.* doi:[10.1002/aenm.201100713](https://doi.org/10.1002/aenm.201100713)
48. Razaq A, Nyholm L, Sjödin M, Strømme M, Mihranyan A (2012) *Adv Energy Mater.* doi:[10.1002/aenm.201100713](https://doi.org/10.1002/aenm.201100713)
49. Mihranyan A, Llagostera AP, Karmhag R, Strømme M, Ek R (2004) *Int J Pharm* 269:433. doi:[10.1016/j.ijpharm.2003.09.030](https://doi.org/10.1016/j.ijpharm.2003.09.030)
50. Pääkkö M, Ankerfors M, Kosonen H et al (2007) *Biomacromolecules* 8:1934. doi:[10.1039/b810371b](https://doi.org/10.1039/b810371b)
51. Segal L, Creely JJ, Martin AE Jr, Conrad CM (1959) *Text Res J* 29:786
52. ASTM-D-1795-96 (2007) Standard test method for intrinsic viscosity of cellulose. doi:[10.1520/D1795-96R07E01](https://doi.org/10.1520/D1795-96R07E01)
53. Okita Y, Saito T, Isogai A (2010) *Biomacromolecules* 11:1696. doi:[10.1021/bm100214b](https://doi.org/10.1021/bm100214b)
54. Driemeier C, Calligaris GA (2011) *J Appl Cryst* 44:184. doi:[10.1107/S0021889810043955](https://doi.org/10.1107/S0021889810043955)
55. Battista OA (1950) *Ind Eng Chem* 42:502. doi:[10.1021/ie50483a029](https://doi.org/10.1021/ie50483a029)
56. Ek R, Gustafsson C, Nutt A, Iversen T, Nyström C (1998) *J Mol Recognit* 11:263. doi:[10.1002/\(SICI\)1099-1352\(199812\)11:1/6<263::AID-JMR437>3.0.CO;2-G](https://doi.org/10.1002/(SICI)1099-1352(199812)11:1/6<263::AID-JMR437>3.0.CO;2-G)
57. Rowe RC, Sheskey PJ, Quinn ME (2009) *Handbook of pharmaceutical excipients*. Pharmaceutical Press, London
58. Henriksson M, Berglund LA, Isaksson P, Lindström T, Nishino T (2008) *Biomacromolecules* 9:1579. doi:[10.1021/bm800038n](https://doi.org/10.1021/bm800038n)
59. Sasso C, Bruyant N, Beneventi D et al (2011) *Cellulose* 18:1455. doi:[10.1007/s10570-011-9583-2](https://doi.org/10.1007/s10570-011-9583-2)